American Mineralogist, Volume 96, pages 423–429, 2011

Fluorphosphohedyphane, $Ca_2Pb_3(PO_4)_3F$, the first apatite supergroup mineral with essential Pb and F

Anthony R. Kampf[1,*] and Robert M. Housley[2]

[1]Mineral Sciences Department, Natural History Museum of Los Angeles County, 900 Exposition Blvd., Los Angeles, California 90007, U.S.A.
[2]Division of Geological and Planetary Sciences, California Institute of Technology, Pasadena, California 91125, U.S.A.

Abstract

The new mineral fluorphosphohedyphane, $Ca_2Pb_3(PO_4)_3F$, the F-analog of phosphohedyphane, is hexagonal with space group $P6_3/m$ and cell parameters a = 9.6402(12), c = 7.0121(8) Å, V = 564.4(1) Å^3, and Z = 2. It occurs in the oxidation zone of a small Pb-Cu-Zn-Ag deposit, the Blue Bell claims, about 11 km west of Baker, San Bernardino County, California. It forms as sub-parallel intergrowths and irregular clusters of transparent, colorless, highly lustrous, hexagonal prisms with pyramidal terminations. It is found in cracks and narrow veins in a highly siliceous hornfels in association with cerussite, chrysocolla, fluorite, fluorapatite, goethite, gypsum, mimetite, opal, phosphohedyphane, plumbogummite, plumbophyllite, plumbotsumite, pyromorphite, quartz, and wulfenite. The streak of the new mineral is white, the luster is subadamantine, and the Mohs hardness is about 4. The mineral is brittle with subconcoidal fracture and no cleavage. The calculated density is 5.445 g/cm^3 based upon the empirical formula. Optical properties (589 nm): uniaxial (–), ω = 1.836(5), ε = 1.824(5), nonpleochroic. SEM-EDS analyses yielded the averages and ranges in wt%: O 21.28 (20.31–22.14), F 1.59 (1.38–1.91), P 10.33 (9.81–10.83), Ca 9.66 (8.97–10.67), Pb 60.08 (57.67–61.21), total 102.95 (102.02–103.88), providing the empirical formula (based on P = 3): $Ca_{2.00}(Pb_{2.61}Ca_{0.17})_{\Sigma 2.78}P_3O_{11.91}F_{0.75}$. Infrared spectroscopy showed no evidence of OH or carbonate. The strongest powder X-ray diffraction lines are [d(*hkl*)I]: 8.38(100)22, 3.974(111)28, 3.506(002)25, 2.877(121,211)100, 1.878(213,123)26. Fluorphosphohedyphane has the apatite structure (R_1 = 1.75% for 444 reflections with $F_o > 4\sigma F$) with ordering of Ca and Pb in two cation sites, as in hedyphane and phosphohedyphane. The Pb^{2+} cation exhibits a stereoactive $6s^2$ lone-electron-pair. The X anion site at (0, 0, ½) is fully occupied by F forming six bonds of 2.867 Å to Pb atoms, in contrast to the six Pb-Cl bonds of 3.068 Å in phosphohedyphane.

Keywords: Fluorphosphohedyphane, new mineral, crystal structure, apatite supergroup, hedyphane group, Pb^{2+} $6s^2$ lone-electron-pair, Blue Bell claims, California

Introduction

The minerals of the apatite supergroup (with the apatite structure) have the general formula $M1_2M2_3(TO_4)_3X$, where M1 is a nine-coordinated (or 6+3 coordinated) cation site, M2 is a seven-coordinated cation site, T is a tetrahedral site, and X is an anion site occupied by Cl^-, F^-, or OH^- (Pasero et al. 2010). Phosphohedyphane, $Ca_2Pb_3(PO_4)_3Cl$, was described by Kampf et al. (2006), who noted it to be the ordered intermediate between chlorapatite, $Ca_5(PO_4)_3Cl$, and pyromorphite, $Pb_5(PO_4)_3Cl$. They showed it to be a fairly widespread phase, occurring at the type locality, the Capitana mine, Copiapó, Chile, as well as 16 other localities worldwide. Since that time, the mineral has been found by us and others at numerous other localities (e.g., Birch and Mills 2007).

Pyromorphite is an even more widespread phase; however the F analog of pyromorphite has not as yet been found in nature and, although the OH analog has been reported by several sources (e.g., Temple 1956), it has not been approved as a mineral. The prevalence of pyromorphite as opposed to its F- and OH-analogs may be related to the presence of lead as the dominant cation at both the M1 and M2 sites of the apatite structure, which results in larger unit-cell dimensions and makes Cl^-, whose ionic radius is markedly greater than those of F^- and OH^-, the best candidate to occupy the X site. Similarly, F- and OH-analogs of phosphohedyphane have not been previously reported, although Stalder and Rozendaal (2002) report a "calcian pyromorphite" that is very low in Cl and F, which may correspond to the OH-analog of phosphohedyphane. Herein, we report the first occurrence of the F-analog of phosphohedyphane from the Blue Bell claims, near Baker, San Bernardino County, California. It is the first naturally occurring phase with the apatite structure that contains both Pb and F as essential constituents.

The new mineral was originally approved by the Commission on New Minerals, Nomenclature and Classification of the International Mineralogical Association (IMA 2008-068) with the name phosphohedyphane-(F); however, this was changed to fluorphosphohedyphane in accord with the new nomenclature

* E-mail: akampf@nhm.org

scheme for the apatite supergroup (Pasero et al. 2010). Six cotype specimens are deposited in the Natural History Museum of Los Angeles County under catalog numbers 60550, 60551, 60552, 60553, 60554, and 60555.

Occurrence

The Blue Bell claims, which exploit the oxidation zone of a small Pb-Cu-Zn-Ag deposit, consist of a group of mostly small workings and one longer branching adit, all located on small Joe Dandy Hill in the SW¼ of section 2, T13N, R7E in the Soda Mountains (35°14′31″N, 116°12′17″W), about 11 km west of Baker, San Bernardino County, California, U.S.A. Historical and geological background for the deposit is provided by Kampf et al. (2009).

Fluorphosphohedyphane is found in an adit, referred to as the C adit, in cracks and narrow veins in a highly siliceous quartzite-like hornfels in a fractured and chaotic region of limestone showing irregular skarn formation. These cracks appear to have initially been largely filled with cerussite, silica, and/or chrysocolla. Species observed in direct association with fluorphosphohedyphane include cerussite, chrysocolla, fluorite, fluorapatite, goethite, gypsum, mimetite, opal, phosphohedyphane, plumbogummite, plumbophyllite, plumbotsumite, quartz, and wulfenite. Other species identified nearby include beudantite, boleite, calcite, celestine, creaseyite, dioptase, ferrisurite, hemimorphite, mottramite, sepiolite, and vanadinite. The conditions of formation must have been neutral to basic because fluorphosphohedyphane is unstable in even weak acids.

Physical and optical properties

Fluorphosphohedyphane forms hexagonal prisms with pyramidal terminations. Forms observed are {100} and {101} (Fig. 1). Individual crystals are up to about 0.5 mm in length and 0.1 mm in diameter, and are commonly doubly terminated. Crystals often occur in sub-parallel intergrowths and irregular clusters.

Crystals are colorless and transparent with subadamantine luster. The high luster is useful in discriminating fluorphosphohedyphane from fluorapatite, which occurs in otherwise very similar crystals. The streak is white and the Mohs hardness is about 4. The fracture is subconchoidal, the tenacity is brittle and no cleavage or parting was observed. The mineral is non-fluorescent. Density could not be measured because the density is greater than available high-density liquids and there is insufficient material for physical measurement. The density calculated based on the empirical formula and single-crystal cell is 5.445 g/cm^3.

The mineral is optically uniaxial (–) with optical constants measured in sodium light (589 nm): ε = 1.836(5) and ε = 1.824(5). No pleochroism was observed. The Gladstone-Dale compatibility index $1 - (K_P/K_C)$ as defined by Mandarino (1981) provides a measure of the consistency among the average index of refraction, calculated density and chemical composition. For fluorphosphohedyphane, the compatibility index is 0.009, indicating superior agreement among these data.

Infrared spectroscopy

Attenuated total reflectance (ATR) infrared (IR) spectra were obtained with a Thermo-Nicolet Magna 860 FTIR operating at 4 cm^{-1} resolution and utilizing a SensIR Durascope accessory with a diamond sample plate. Small quantities of samples were selected for purity under a binocular microscope, transferred to a small boron carbide mortar and pestle and ground to a fine powder. A quantity of powdered sample sufficient to cover about a 1 mm diameter area on the ATR's diamond plate was first used to obtain maximum sensitivity in looking for the possible presence of OH. The spectrum obtained for the wavelength range 4000 to 1400 cm^{-1} was essentially featureless with no evidence of the typical OH band near 3550 cm^{-1}.

Some of the sample was then diluted with KBr to reduce saturation broadening of the absorption lines and run against a KBr powder background. After correcting for a modest slope in the background, the resulting spectrum for the range 1400 to 400 cm^{-1} is shown in Figure 2. Comparison of this spectrum to the ATR-IR spectrum of a pure pyromorphite in the RRUFF database (http://rruff.info; Downs 2006) shows that all of the absorption bands in the fluorphosphohedyphane spectrum are shifted to slightly higher energies. This is probably due to the substitution of Ca for some of the heavier Pb.

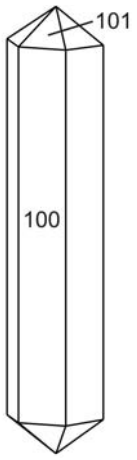

Figure 1. Crystal drawing of fluorphosphohedyphane (clinographic projection).

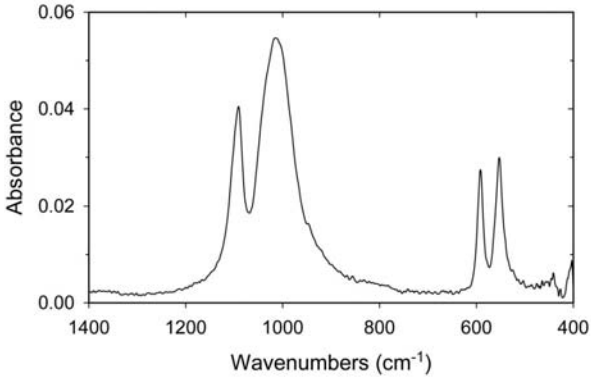

Figure 2. ATR-IR spectrum of fluorphosphohedyphane diluted in KBr.

CHEMISTRY

Numerous matrix specimens and detached crystal groups of apatite and hedyphane group minerals from the C adit of the Blue Bell claims were examined by SEM/EDS during the early part of this study using a Philips XM30 FESEM equipped with an ETEC backscattered electron detector, an IMIX thin-window detector and an INCA EDS analysis system. Species identified include fluorapatite, mimetite, pyromorphite, vanadinite, phosphohedyphane, and fluorphosphohedyphane. Compositions were noted between pyromorphite and mimetite and between pyromorphite and phosphohedyphane, but none were found between phosphohedyphane and chlorapatite (or fluorapatite). This is consistent with the findings reported by Kampf et al. (2006) in their EDS survey of the pyromorphite–mimetite–turneaureite–chlorapatite system. Some crystals and crystal groups exhibited complex zonation and overgrowths or intergrowths of pyromorphite, phosphohedyphane, fluorapatite, and fluorphosphohedyphane; however, no zones with mixed contents of F and Cl were observed.

Two polished microprobe sections were made and carbon coated. One contained several small crystals and crystal groups from the general area of the fluorphosphohedyphane occurrence in the C adit. The other contained only crystals from the same co-type specimen (60553) that yielded the fluorphosphohedyphane crystal used in the structure study. Both sections also contained fluorite and cerussite as internal standards. The sections were carefully examined in the SEM prior to microprobe analysis. The crystals in the co-type (60553) section contained only fluorphosphohedyphane. A crystal group in the other section contains what appears to be an overgrowth sequence from pyromorphite to phosphohedyphane to fluorphosphohedyphane to fluorapatite, but with some corrosion and fracturing between phases. Backscatter electron (BSE) imaging revealed light/dark zoning in both the phosphohedyphane and the fluorphosphohedyphane. SEM-EDS analyses demonstrated that the brightness contrast is related to the Pb/Ca ratios. Figure 3 illustrates this zoning in several intergrown fluorphosphohedyphane crystals.

Optimized SEM-EDS analyses were done using the internal cerussite standard for Pb and O and the internal fluorite standard for Ca and F, along with stored standards of GaP for P and KCl for Cl. These showed that in fluorphosphohedyphane Pb/Ca ranges from near the ideal of 1.50 (corresponding to Ca_2Pb_3) in light zones down to about 1.2 in the more volumetrically important dark zones. On the other hand, in phosphohedyphane Pb/Ca is always higher than the ideal 1.5 ratio. Phosphohedyphane always exhibited close to one Cl apfu. All of the crystals examined from the area near the crystal used for the structure analysis had only fluorphosphohedyphane chemistry, with dark regions strongly dominant over light regions. The crystal used for the structure analysis exhibited no visual evidence of zoning when examined using a petrographic microscope.

Analyses of the crystals in the section with the co-type (60553) material were conducted in WDS mode on a JEOL8200 microprobe using a 15 kV focused electron beam at 25 nA. Probe standards were pyromorphite for Pb, apatite for Ca and P and synthetic fluorophlogopite for F. Four analyses conducted on dark BSE regions provided the following averages and ranges in wt%: CaO 13.43 (12.98–13.74), PbO 61.69 (61.24–62.23), P_2O_5 22.88 (22.60–23.16), F 2.19 (2.02–2.52), O≡F –0.92, total 99.27 wt%. Four analyses of light BSE regions provided: CaO 11.21 (10.56–11.89), PbO 64.03 (63.05–64.99), P_2O_5 22.44 (22.16–23.18), F 1.08 (0.82–1.43), O≡F –0.45, total 98.31 wt%. No other elements were seen in the EDS study. In the microprobe run, As, V, Cl, Si, and Sr were below detection limits. The empirical formula derived from the averaged EMP analyses of the dark BSE regions (based on P = 3) is $Ca_2(Pb_{2.57}Ca_{0.23})_{\Sigma 2.80}(P_3O_{11.76})F_{1.07}$.

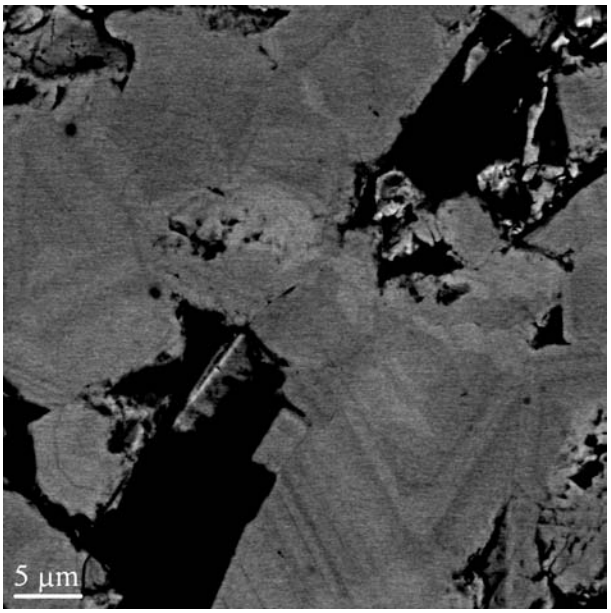

FIGURE 3. BSE image exhibiting light/dark zoning in fluorphosphohedyphane. The light zones correspond to higher Pb/Ca ratios.

Stormer et al. (1993) reported that, when conducting EMP analyses of F in apatite, diffusion of F to the sample surface can yield values that are up to 100% too high. Because the EMP methods recommended by those authors could not be used for our small zoned samples, we investigated the possibility of obtaining good F analyses using SEM-EDS. After verifying that a focused SEM beam, even with its much lower current, caused F analyses to increase by approximately a factor of 2 within 3 min, we determined that, with the beam scanning over a 5 µm square area, there was no change in F values over 30 min.

We used this method to obtain eleven 50 s analyses of a uniformly dark single crystal in the section with the co-type (60553) material. These analyses yielded the following averages and ranges in wt%: O 21.28 (20.31–22.14), F 1.59 (1.38–1.91), P 10.33 (9.81–10.83), Ca 9.66 (8.97–10.67), Pb 60.08 (57.67–61.21), total 102.95 (102.02–103.88), providing the empirical formula (based on P = 3): $Ca_{2.00}(Pb_{2.61}Ca_{0.17})_{\Sigma 2.78}P_3O_{11.96}F_{0.75}$, which can be charge balanced by adjusting the O content slightly yielding $Ca_{2.00}(Pb_{2.61}Ca_{0.17})_{\Sigma 2.78}P_3O_{11.91}F_{0.75}$. This is very close to that derived from the EMP analyses, except for having about 30% lower F, and we consider this to be a truer reflection of the chemical composition of the dark regions that correspond to the volumetrically most important portions of the fluorphospho-

hedyphane crystals. The simplified formula is $Ca_2Pb_3(PO_4)_3F$, which requires CaO 11.15, PbO 66.58, P_2O_5 21.17, F 1.89, less O=F –0.80, total 100.00 wt%.

Fluorphosphohedyphane decomposes quickly in dilute HCl and the residue dissolves slowly.

X-RAY CRYSTALLOGRAPHY AND STRUCTURE DETERMINATION

Both powder and single-crystal X-ray diffraction data were obtained on a Rigaku R-Axis Rapid II curved imaging plate microdiffractometer utilizing monochromatized Mo*K*α radiation. The powder data presented in Table 1 show good agreement with the pattern calculated from the structure determination.

The Rigaku CrystalClear software package was used for processing of the structure data. The SHELXL-97 software (Sheldrick 2008) was used for the refinement of the structure. The atomic coordinates of phosphohedyphane (apatite structure type) were used as the starting point. The F is located at (0, 0, ½), as is Cl in phosphohedyphane. Efforts to place the F atom at a half-occupied site along (0, 0, *z*) were unsuccessful and, with F located at (0, 0, ½), the largest electron density residual along (0, 0, *z*) is 0.43 *e*/A^3 at (0, 0, 0.374). Although the F site refined best at full occupancy, its relatively high-displacement parameters [e.g., U_{eq} = 0.057(3)] are consistent with less than full occupancy, as is suggested by the chemical analyses, which indicate 0.75 F apfu.

TABLE 1. Observed and calculated X-ray powder-diffraction data for fluorphosphohedyphane

I_{obs}	d_{obs}	d_{calc}	I_{calc}	*hkl*
20	8.384(8)	8.3486	24	100
5	4.83(2)	4.8201	6	110
6	4.182(6)	4.1743	6	200
26	3.978(1)	3.9721	29	111
23	3.509(1)	3.5060	25	002
12	3.239 (3)	3.2326	12	102
15	3.161(2)	3.1555	10,8	210,120
100	2.8805(7)	2.8776	51,49	211,121
8	2.81(1)	2.8353	17	112
		2.7829	7	300
17	2.3485(9)	2.3454	10,3	122,212
20	2.0981(3)	2.1031	12	113
		2.0872	10	400
8	1.9872(4)	1.9861	10	222
13	1.9332(9)	1.9322	4	
26	1.8792(3)	1.8782	16,14	123,213
12	1.8488(6)	1.8476	9,6	231,321
14	1.8223(6)	1.8218	8,3	410,140
13	1.7930(2)	1.7934	18	402
8	1.7518(5)	1.7530	7	004
4	1.6742(4)	1.6697	3	500
4	1.6169(3)	1.6166	3,1	412,142
10	1.5664(3)	1.5661	10	331
6	1.5338(5)	1.5324	3,2	124,214
6	1.5073(3)	1.5075	8	502
10	1.4820(4)	1.4815	3,3	233,323
5	1.4623(3)	1.4663	2,3	151,511
		1.4606	4	332
8	1.3435(2)	1.3424	5	404
5	1.324(1)	1.3241	5	333
4	1.312(2)	1.3132	4,1	521,251
13	1.2814(3)	1.2816	4,4	125,215
10	1.2630(2)	1.2632	4,2	414,144
5	1.2510(2)	1.2527	4,2	161,611

Notes: I_{obs} and d_{obs} derived by profile fitting using JADE 9.1 software. I_{calc} and d_{calc} calculated from the crystal structure using Powder Cell (Kraus and Nolze 1996). Unit-cell parameters refined from the powder data using JADE 9.1 with whole pattern fitting are: a = 9.632(1) and c = 7.010(1) Å.

The refinement indicated that the M1(4*f*) site at (1/3, 2/3, 0.0059) is fully occupied by Ca and the site M2(6*h*) site at (0.23955, 0.00861, 1/4) is dominated by Pb. Slightly less than full occupancy is indicated at the M2 site. With only Pb assigned to the site, the occupancy refines to 87% (2.61 Pb per formula unit) with R_1 = 0.0176. With the occupancy of this site assigned 85.6% Pb and 7.7% Ca corresponding to 2.61 Pb and 0.26 Ca, as indicated in the empirical formula, the R_1 goes up slightly to 0.0179. Ultimately, we decided that the best approach was to refine the Pb and Ca occupancies at the site with full total occupancy. This yielded 0.882(7) Pb and 0.118(7) Ca on the site, corresponding to 2.65 Pb and 0.35 Ca apfu, with R_1 = 0.0175.

The details of the data collection and structure refinement are provided in Table 2. The final atomic coordinates and displacement parameters are in Table 3. Selected interatomic distances are listed in Table 4 and bond valences in Table 5. Structure factors and CIF are on deposit[1] with MSA.

DESCRIPTION OF THE STRUCTURE

Fluorphosphohedyphane has a $P6_3/m$ apatite structure (Fig. 4) with Ca and Pb ordered in the two nonequivalent large cation sites. The M1(4*f*) site is completely and fully occupied by Ca and the M2(6*h*) site is occupied predominantly by Pb. Similar ordering has been reported in phosphohedyphane (Kampf et al. 2006), hedyphane (Rouse et al. 1984), and the synthetic OH-analog of phosphohedyphane (Engel et al. 1975), as well as in numerous other minerals and synthetic compounds with the apatite structure (Pasero et al. 2010).

[1] Deposit item AM-11-006, Structure factors and CIF. Deposit items are available two ways: For a paper copy contact the Business Office of the Mineralogical Society of America (see inside front cover of recent issue) for price information. For an electronic copy visit the MSA web site at http://www.minsocam.org, go to the *American Mineralogist* Contents, find the table of contents for the specific volume/issue wanted, and then click on the deposit link there.

TABLE 2. Data collection and structure refinement details for fluorphosphohedyphane

Diffractometer	Rigaku R-Axis Rapid II
X-ray radiation/power	Mo*K*α (λ = 0.71075 Å)/50 kV, 40 mA
Temperature	298(2) K
Structural formula	$Ca_2(Pb_{2.65}Ca_{0.35})(PO_4)_3F$
Space group	$P6_3/m$
Unit-cell dimensions	a = 9.6402(12) Å
	c = 7.0121(8) Å
Z	2
Volume	564.4(1) Å^3
Density (for structural formula)	5.573 g/cm^3
Absorption coefficient	40.945 mm^{-1}
F(000)	828
Crystal size	95 × 25 × 25 µm
θ range	3.79 to 27.42°
Index ranges	$-12 \le h \le 12$, $-12 \le k \le 12$, $-9 \le l \le 9$
Reflections collected/unique	13559/459 [R_{int} = 0.0419]
Reflections with $F_o > 4\sigma F$	444
Completeness to θ = 27.46°	98.1%
Max. and min. transmission	0.4276 and 0.1122
Refinement method	Full-matrix least-squares on F^2
Parameters refined	41
GoF	1.229
Final R indices [$F_o > 4\sigma F$]	R_1 = 0.0175, wR_2 = 0.0334
R indices (all data)	R_1 = 0.0186, wR_2 = 0.0338
Extinction coefficient	0.00036(11)
Largest diff. peak/hole	+0.700/–1.452 *e*/A^3

Notes: $R_{int} = \Sigma|F_o^2 - F_o^2(\text{mean})|/\Sigma[F_o^2]$. GoF = $S = \{\Sigma[w(F_o^2 - F_c^2)^2]/(n-p)\}^{1/2}$. $R_1 = \Sigma||F_o| - |F_c||/\Sigma|F_o|$. $wR_2 = \{\Sigma[w(F_o^2 - F_c^2)^2]/\Sigma[w(F_o^2)^2]\}^{1/2}$. $w = 1/[\sigma^2(F_o^2) + (aP)^2 + bP]$ where a is 0, b is 5.6001, and P is $[2F_c^2 + \text{Max}(F_o^2,0)]/3$.

TABLE 3. Atomic coordinates and displacement parameters (Å²) for fluorphosphohedyphane

	x	*y*	*z*	U_{eq}	U_{11}	U_{22}	U_{33}	U_{23}	U_{13}	U_{12}
Ca1	0.3333	0.6667	0.0046(3)	0.0085(4)	0.0093(5)	0.0093(5)	0.0068(8)	0.0	0.0	0.0047(3)
Pb2*	0.23960(3)	0.00873(3)	0.25	0.0118(1)	0.0099(2)	0.0094(2)	0.0149(2)	0.0	0.0	0.0038(1)
P	0.4183(2)	0.3880(2)	0.25	0.0099(5)	0.0101(9)	0.0076(8)	0.0120(10)	0.0	0.0	0.0043(7)
O1	0.3592(6)	0.5078(6)	0.25	0.016(1)	0.020(3)	0.014(3)	0.016(3)	0.0	0.0	0.011(2)
O2	0.6047(6)	0.4731(6)	0.25	0.016(1)	0.011(2)	0.016(3)	0.024(3)	0.0	0.0	0.007(2)
O3	0.3610(5)	0.2780(4)	0.0733(6)	0.0188(9)	0.029(2)	0.016(2)	0.017(2)	−0.005(2)	−0.007(2)	0.014(2)
F	0.0	0.0	0.5	0.057(3)	0.048(4)	0.048(4)	0.076(9)	0.0	0.0	0.024(2)

* The refined Pb:Ca site occupancy of the Pb2 (M2) site is 0.882(7):0.118(7).

TABLE 4. Selected bond distances (Å) for fluorphosphohedyphane

Ca1-O1 (×3)	2.398(4)
Ca1-O2 (×3)	2.483(4)
Ca1-O3 (×3)	2.774(4)
<Ca1-O>	2.552
Pb2-O2	2.407(5)
Pb2-O3 (×2)	2.527(4)
Pb2-O3 (×2)	2.570(4)
Pb2-F (×2)	2.8672(3)
Pb2-O1	3.200(5)
Pb2-O3 (×2)	3.581(4)
<Pb2-O>	2.870
P-O1	1.523(5)
P-O3 (×2)	1.542(4)
P-O2	1.558(5)
<P-O>	1.541

TABLE 5. Bond-valence analysis for fluorphosphohedyphane

	O1	O2	O3	F	Sum
Ca1	0.312 ×3→	0.248 ×3→	0.113 ×3→		2.019
		×2↓	×2↓		
Pb2*	0.075	0.392	0.305 ×2→	0.099	1.899
			0.278 ×2→	×2→ ×6↓	
			0.034 ×2→		
P	1.245	1.132	1.182 ×2→		4.741
Sum	1.943	2.020	1.912	0.594	

Notes: Values are expressed in valence units. Multiplicity is indicated by ×→↓; Pb^{2+}-O bond strengths from Krivovichev and Brown (2001); Pb^{2+}-F and P^{5+}-O bond strengths from Brese and O'Keeffe (1991); Ca^{2+}-O and Ca^{2+}-F bond strengths from Brown and Altermatt (1985).

* Based on $Pb_{0.88}Ca_{0.12}$

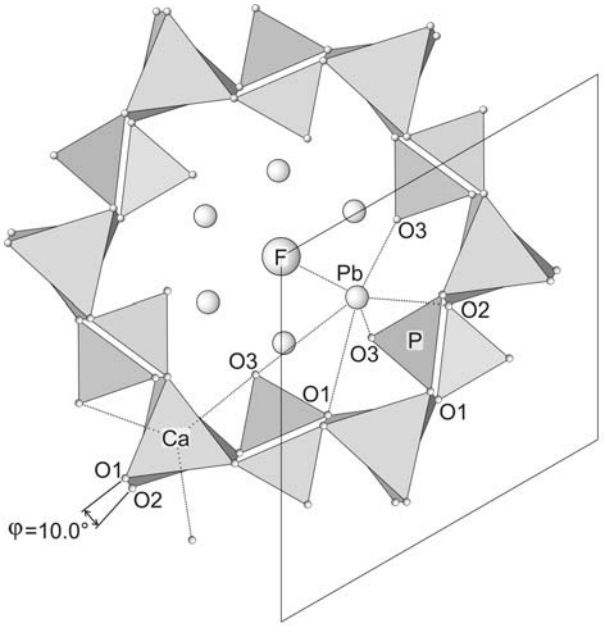

FIGURE 4. Fluorphosphohedyphane crystal structure viewed down [001]. Pb-O,F and Ca-O3 bonds are shown by dotted lines. The metaprism twist angle, φ, is also shown.

The M1 site

The ability of the apatite structure to accommodate a wide variety of cations is well known. The M1 and M2 sites can accommodate the same cations; however, they have quite distinct coordinations. The M1 site is surrounded by three O1 (at 2.398 Å in fluorphosphohedyphane) and three O2 atoms (at 2.483 Å in fluorphosphohedyphane) forming a twisted trigonal prism that can be regarded as intermediate between a trigonal prism and an octahedron. In addition, three more distant equatorial O3 atoms (at 2.774 Å in fluorphosphohedyphane) yield a tri-capped trigonal prism. The twisted trigonal prism has also been referred to as a "metaprism" (White and Dong 2003; Dong and White 2004a, 2004b; Mercier et al. 2005). The amount of twisting of the metaprism, referred to as the metaprism twist angle (φ), is the angle O1-Ca1-O2 projected on (001). The metaprism twist angle theoretically ranges from 0° (for a trigonal prism) to 60° (for an octahedron). Actual metaprism twist angles in apatite structures vary from 5.2° to 26.7° (White and Dong 2003). The apatite structure can be regarded as a framework made up of tetrahedra and M1 metaprisms forming channels along **c** in which the M2 cations and halide or hydroxyl anions are located (White et al. 2005). Smaller metaprism twist angles yield larger M1 sites and larger diameter channels.

When both the M1 and M2 sites are occupied by the same cations or by cations of roughly the same size, the metaprism twist angle tends to be relatively large, e.g., pyromorphite, "lead fluorapatite" [$Pb_5(PO_4)_3F$] (Fleet et al. 2010), and fluorapatite have twist angles of 17.6°, 21.7°, and 23.3°, respectively. When a smaller cation, such as Ca^{2+}, is in the M1 site and a larger cation, such as Pb^{2+}, is in the M2 site, the metaprism twist angle must be relatively small to allow the framework to expand to accommodate the larger M2 cation in the channel. For fluorphosphohedyphane, phosphohedyphane, and hedyphane, in which Ca^{2+} occupies the M1 site and Pb^{2+} occupies the M2 site, the M1 metaprism twist angles are notably smaller, 10.0°, 8.6°, and 5.2°, respectively.

The M2 site

The M2 site coordination in apatite structures is quite variable, being dependent on the cation in the site, the channel diameter and the identity (and placement) of the channel anion (OH^-, F^-, Cl^-, etc.). The ability of the M2 site to accommodate both larger and lopsided coordinations accounts for the strong preference of Pb^{2+}, with stereoactive $6s^2$ lone-electron-pairs, for this site (Rouse et al. 1984; Kampf et al. 2006). In fluorphosphohedyphane, phosphohedyphane, and hedyphane, the M2 site, occupied predominantly by Pb, exhibits very similar lopsided 10-fold coordinations to eight O atoms and two X (Cl or F) atoms (Fig. 5). The Pb-O bonds consist of one very

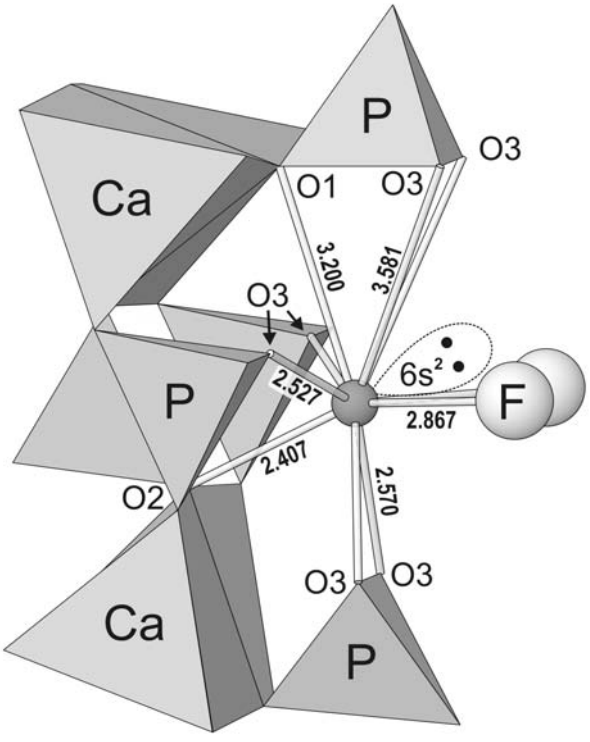

FIGURE 5. The Pb coordination in fluorphosphohedyphane viewed slightly canted from down the **c**-axis. The likely approximate location of the Pb^{2+} $6s^2$ lone-electron-pair is shown.

short bond to O2 (at 2.407 Å in fluorphosphohedyphane), four somewhat longer bonds to O3 [at 2.527 (×2) and 2.570 (×2) Å in fluorphosphohedyphane], one moderately long bond to O1 (at 3.200 Å in fluorphosphohedyphane), and two very long bonds to O3 [at 3.581 (×2) Å in fluorphosphohedyphane]. Note that a long Pb-O1 distance (at 3.453 Å in fluorphosphohedyphane) should not be considered a bond because it is on the same side of the coordination as the shortest Pb-O bonds. The two bonds to X are relatively short (for Pb-Cl) in hedyphane (3.117 Å) and phosphohedyphane (3.0679 Å) and relatively long (for Pb-F) in fluorphosphohedyphane (2.8672 Å).

The X anion site

The role of the channel anion (X = OH^-, F^-, Cl^-) in apatite structures has been extensively studied (e.g., Hughes et al. 1989; Kim et al. 2000). This anion assumes positions at the center of the channel at (0, 0, *z*), where it is coordinated to either three or six cations in the surrounding M2 sites. The interaction between the channel anion and the cations in the M2 sites dictates the position of the anion. In fluorapatite, the relatively small F^- anion is situated on a mirror plane at (0, 0, ¼) at the center of a triangle formed by three Ca^{2+} cations. In chlorapatite, the larger size of the Cl^- anion "forces" it to assume a position significantly displaced from the mirror plane toward the special position at (0, 0, ½). Kim et al. (2000) provide its location as (0, 0, 0.439), where it may also participate in relatively long bonds to three additional Ca^{2+} cations in M2 sites. In most instances, the Cl^- anions are disordered in half-occupied sites above and below the mirror plane and the $P6_3/m$ space group is retained; however, in some cases the Cl^- anions are ordered resulting in a monoclinic structure ($P2_1/b$).

The natural and synthetic "lead apatites" are quite different with respect to the placement of the X anion. In pyromorphite (Dai and Hughes 1989), mimetite (Calos and Kennard 1990), hedyphane (Rouse et al. 1984), and phosphohedyphane (Kampf et al. 2006), the Cl^- anions are located at (0, 0, ½), midway between two triangles formed by Pb^{2+} cations in the M2 sites. Each Cl^- anion bonds to six Pb^{2+} cations in a nearly perfect octahedral configuration. Despite the much smaller size of F^-, it too is generally located at (0, 0, ½) in the "lead apatites" (Kim et al. 2000), and such is also the case in fluorphosphohedyphane. Kim et al. (2000) attribute the placement of Cl^- and F^- at (0, 0, ½) to the stereoactive Pb^{2+} $6s^2$ lone-electron-pairs, which they interpret as projecting into the voids at the center of the Pb^{2+} triangles (at 0, 0, ¼), thereby forcing the halide ions away from the center of these triangles (see Fig. 5).

An interesting consequence of the constraint imposed on the halide ions by placing them at (0, 0, ½) is that their bond lengths to the surrounding six Pb^{2+} cations are constrained to far from ideal values. In the case of phosphohedyphane, this results in much shorter than ideal Pb-Cl bonds and a much higher than optimal bond-valence sum for Cl^- of 1.402 vu (Kampf et al. 2006). In the case of fluorphosphohedyphane, this results in much longer than ideal Pb-F bonds and a much lower than optimal bond-valence sum for F^- of 0.594 vu (Table 5). It is noteworthy that, in the structure of synthetic "lead fluorapatite" [$Pb_5(PO_4)_3F$] (Fleet et al. 2010), the F^- anion is at (0, 0, 0.461), rather than (0, 0, ½); however, the Pb–F bonds of 2.75 (×3) and 3.11 Å (×3) are also significantly longer than normal, presumably because of the lone-pair effect, yielding a bond-valence sum for the F^- of 0.593 vu, practically identical to that found in fluorphosphohedyphane.

ACKNOWLEDGMENTS

John M. Hughes and Stuart J. Mills provided helpful comments on the manuscript. Associate Editor, Rhian Jones is especially thanked for pointing out the need to look more critically at the F analyses. Joseph Marty of Salt Lake City, Utah, is thanked for providing the specimens of fluorphosphohedyphane used in this study. The IR spectroscopy was conducted in the laboratory of George R. Rossman at the California Institute of Technology and with his assistance. The SEM/EDS studies and the microprobe analyses were supported by a grant to Caltech from the Northern California Mineralogical Association. The remainder of this study was funded by the John Jago Trelawney Endowment to the Mineral Sciences Department of the Natural History Museum of Los Angeles County.

REFERENCES CITED

Birch, W.D. and Mills, S.J. (2007) Sulphide-carbonate reaction in recrystallized limestone at Lilydale, Victoria, Australia: A new occurrence of phosphohedyphane. Australian Journal of Mineralogy, 13, 73–82.

Brese, N.E. and O'Keeffe, M. (1991) Bond-valence parameters for solids. Acta Crystallographica, B47, 192–197.

Brown, I.D. and Altermatt, D. (1985) Bond-valence parameters obtained from a systematic analysis of the inorganic crystal structure database. Acta Crystallographica, B41, 244–247.

Calos, N.J. and Kennard, C.H.L. (1990) Crystal structure of mimetite, $Pb_5(AsO_4)_3Cl$. Zeitschrift für Kristallographie, 191, 125–129.

Dai, Y. and Hughes, J.M. (1989) Crystal structure refinements of vanadinite and pyromorphite. Canadian Mineralogist, 27, 189–192.

Dong, Z.L. and White, T.J. (2004a) Calcium-lead fluoro-vanadinite apatites: I. Disequilibrium structures. Acta Crystallographica, B60, 138–145.

——— (2004b) Calcium-lead fluoro-vanadinite apatites: II. Equilibrium structures. Acta Crystallographica, B60, 146–154.

Downs, R.T. (2006) The RRUFF Project: an integrated study of the chemistry,

crystallography, Raman and infrared spectroscopy of minerals. Program and Abstracts of the 19th General Meeting of the International Mineralogical Association in Kobe, Japan. O03-13.
Engel, G., Krieg, F., and Reif, G. (1975) Mischkristallbildung und Kationenordnung im System Bleihydroxylapatit-Calciumhydroxylapatit. Journal of Solid State Chemistry, 15, 117–l 26.
Fleet, M.E., Liu, S., and Shieh, S.R. (2010) Structural change in lead fluorapatite at high pressure. Physics and Chemistry of Minerals, 37, 1–9.
Hughes, J.M., Cameron, M., and Crowley, K.D. (1989) Structural variations in natural F, OH, and Cl apatites. American Mineralogist, 74, 870–876.
Kampf, A.R., Steele, I.M., and Jenkins, R.A. (2006) Phosphohedyphane, $Ca_2Pb_3(PO_4)_3Cl$, the phosphate analogue of hedyphane: Description and crystal structure. American Mineralogist, 91, 1909–1917.
Kampf, A.R., Rossman, G.R., and Housley, R.M. (2009) Plumbophyllite, a new mineral from the Blue Bell claims near Baker, San Bernardino County, California. American Mineralogist, 94, 1198–1204.
Kim, J.Y., Fenton, R.R., Hunter, B.A., and Kennedy, B.J. (2000) Powder diffraction studies of synthetic calcium and lead apatites. Australian Journal of Chemistry, 53, 679–686.
Kraus, W. and Nolze, G. (1996) POWDER CELL—A program for the representation and manipulation of crystal structures and calculation of the resulting X-ray powder patterns. Journal of Applied Crystallography, 29, 301–303.
Krivovichev, S.V. and Brown, I.D. (2001) Are the compressive effects of encapsulation an artifact of the bond valence parameters? Zeitschrift für Kristallographie, 216, 245–247.
Mandarino, J.A. (1981) The Gladstone-Dale relationship: Part IV. The compatibility concept and its application. Canadian Mineralogist, 19, 441–450.
Mercier, P.H.J., Le Page, Y., Whitfield, P.S., Mitchell, L.D., Davidson, I.J., and White, T.J. (2005) Geometrical parameterization of the crystal chemistry of $P6_3/m$ apatites: comparison with experimental data and *ab initio* results. Acta Crystallographica, B61, 635–655.
Pasero, M., Kampf, A.R., Ferraris, C., Pekov, I.V., Rakovan, J., and White, T.J. (2010) Nomenclature of the apatite supergroup minerals. European Journal of Mineralogy, 22, 163–179.
Rouse, R.C., Dunn, P.J., and Peacor, D.R. (1984) Hedyphane from Franklin, New Jersey and Langban, Sweden: Cation ordering in an arsenate apatite. American Mineralogist, 69, 920–927.
Sheldrick, G.M. (2008) A short history of SHELX. Acta Crystallographica, A64, 112–122.
Stalder, M. and Rozendaal, A. (2002) Graftonite in phosphatic iron formations associated with the mid-Proterozoic Zn-Pb deposit, Namaqua province, South Africa. Mineralogical Magazine, 66, 915–927.
Stormer, J.C., Pierson, M.L., and Tacker, R.C. (1993) Variation of F and Cl X-ray intensity due to anisotropic diffusion in apatite during electron microprobe analysis. American Mineralogist, 78, 641–648.
Temple, A.K. (1956) The Leadhills-Wanlockhead lead and zinc deposits. Transactions of the Royal Society of Edinburgh, 63, 85–113.
White, T.J. and Dong, Z.L. (2003) Structural derivation and crystal chemistry of apatites. Acta Crystallographica, B59, 1–16.
White, T.J., Ferraris, C., Kim, J., and Srinivasan, M. (2005) Apatite—An adaptive framework structure. In G. Ferraris and S. Merlino, Eds., Micro- and mesoporous mineral phases, 57, 307–402. Reviews in Mineralogy and Geochemistry, Mineralogical Society of America, Chantilly, Virginia.

MANUSCRIPT RECEIVED APRIL 21, 2010
MANUSCRIPT ACCEPTED SEPTEMBER 9, 2010
MANUSCRIPT HANDLED BY RHIAN JONES